Long-Stroke Hydraulic Robot Motion Control With Incremental Nonlinear Dynamic Inversion

Huang, Yingzhi; Pool, Daan; Stroosma, Olaf; Chu, Qiping

DOI
10.1109/TMECH.2019.2891358

Publication date
2019

Document Version
Accepted author manuscript

Published in
IEEE - ASME Transactions on Mechatronics

Long-Stroke Hydraulic Robot Motion Control with Incremental Nonlinear Dynamic Inversion

Yingzhi Huang, Daan M. Pool, *Member, IEEE,* Olaf Stroosma, QiPing Chu

***Abstract*—High precision motion control of hydraulic manipulators is challenging due to the highly nonlinear dynamics and model uncertainties typical for hydraulic actuators. This paper addresses the implementation of a novel sensor-based Incremental Nonlinear Dynamic Inversion control technique for a high-precision hydraulic force controller in existence of parameter uncertainties. Combined with a widely used force computation outer-loop controller, the proposed motion control structure is implemented on a 6-DOF hexapod hydraulic robot, the SIMONA (Simulation, Motion and Navigation) Research Simulator at TU Delft. The proposed control technique is inherently robust to hydraulic parameter uncertainties. As an important contribution, the robustness against parameter uncertainty is rigorously proven. Stability of the proposed controller is also analysed. Techniques for solving characteristic implementation issues, such as higher-order valve dynamics and oil transmission effects, are discussed in detail. Motion tracking experiment results on the SIMONA simulator validate the effectiveness of the proposed method in terms of performance and the robustness against parameter uncertainties. Significant control accuracy improvement is demonstrated by comparing with the state-of-the-art motion control implementations.**

***Index Terms*—Hydraulic robots, parallel robots, force control, motion control, model uncertainty.**

I. Introduction

HYDRAULIC robotic systems are widely used in heavy-duty machines, legged robots, and vehicle simulator motion systems. They still have higher power-to-weight ratios and inherently higher stiffness and rigidity compared with electrical motors. For applications where high precision control performance is required, such as legged robots control [1], [2], manipulator impedance control [3], [4] and flight simulator motion control [5], high performance controller development is receiving increasing attention in the academia.

One challenge of the hydraulic robot control problem is that hydraulic actuators regard the input as a velocity command, instead of a force command as their electrical counterparts do. This fact prevents the extensively studied general robot control techniques [6]–[9] from direct application, which generally work with force inputs. A few studies successfully implemented model-based control methods based on the integrated mechanics and hydraulic dynamics. Nevertheless, the highly nonlinear hydraulic dynamics have to be significantly simplified by linearization or neglecting leakage or oil compressibility [10], [11]. More importantly, a lack of hydraulic pressure/force controllers largely limits their applications in robot impedance control, vibration isolation and active suspension, where ideal force actuators are generally assumed [12]. One systematic solution for hydraulic systems is cascading the controller into a multi-loop structure, as shown in Fig. 1. An inner-loop hydraulic force controller decouples the hydraulic dynamics from the mechanics, while guiding it to generate the required actuation forces given by the outer-loop motion controller. With a decoupled inner-loop force controller, various advanced (outer-loop) control schemes developed for electrical manipulators become possible to be directly applied to hydraulic robotic systems.

Force control of a hydraulic actuator is challenging due to the highly nonlinear dynamic behavior, and the model uncertainties resulting from model simplification and parameter uncertainty. Meanwhile, as shown in [13], linear controllers (e.g. PID) are fundamentally not capable of achieving high performance for advanced hydraulic force control, since they are severely bandwidth limited in such applications, causing significant phase lag which increases with frequency. This makes more advanced model-based control schemes necessary, such as feedback linearization [3], [14] and its variants, including Nonlinear Dynamic Inversion (NDI) based control [15], Cascade ΔP controller (CdP) [16] and flatness-based control [17]. However, the performance of the feedback linearization based controllers relies on an accurate model and is significantly degraded in existence of parameter mismatches. For linear dynamic inversion, general techniques such as additive-state-decomposition (ASD) have been proposed to deal with model uncertainty and disturbance [18], [19]. When considering the nonlinear hydraulic model uncertainty problem, nonlinear adaptive control is one extensively studied approach [20]–[23]. Among them, as concluded in [24], the most advanced works in terms of motion control accuracy are [22] for hydraulic serial manipulators and [23] for hydraulic parallel robots, each of which provides a stability-guaranteed controller with adaptation of hydraulic parameters. However, in all the mentioned adaptive approaches, the design of the hydraulic parameter adaptation law is coupled with the complete control system design in order to guarantee the stability. It is difficult to directly combine the hydraulic adaptive methods with a different outer-loop controller. Therefore, a high performance, fully decoupled and less model-dependent hydraulic force controller is still to be developed.

Incremental Nonlinear Dynamic Inversion (INDI) [25] is a novel sensor-based nonlinear control technique based on the feedback linearization of the nominal incremental part of the system dynamics. INDI solves the inherent problem of model dependency of traditional feedback linearization. A

The authors are with Control and Simulation Section, Faculty of Aerospace Engineering, Delft University of Technology; Kluyverweg 1, 2629HS, Delft, The Netherlands.

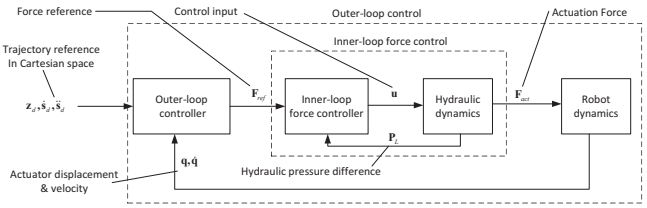

Fig. 1. Cascade-control architecture for hydraulic robots with inner and outer control loops

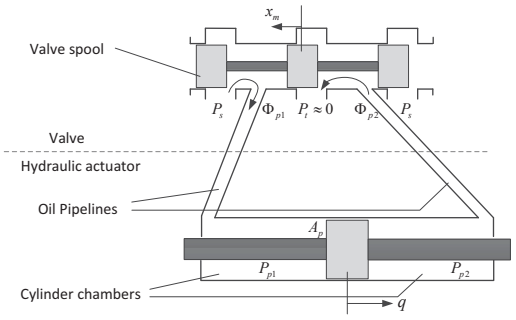

Fig. 2. A valve controlled symmetry hydraulic actuator

number of state-of-the-art nonlinear control applications with INDI have been reported [26], [27], validating the achievable control performance and robustness of INDI towards model uncertainties under the assumption of a high sampling rate. INDI is particularly attractive to high precision force control of hydraulic robots with the following features: 1) Inherently robust to parameter uncertainty and continuous external disturbances, without an explicitly adaptive or robust control algorithm; 2) High control precision with low computation load and straightforward controller design procedures; 3) Achieving precise feedback linearization of highly nonlinear systems without precise knowledge of their dynamics.

In previous reports of this research project, the preliminary theoretical application of INDI was discussed for a single hydraulic actuator model [28] and a hydraulic flight simulator model [29]. However, these simulation studies did not provide any experimental validation. Also, practical issues such as oil pipeline dynamics of long-stroke hydraulic actuators were neglected in the simulation models. Furthermore, none of aforementioned works gave a rigorous proof of the parameter uncertainty resistance features and the stability of INDI.

In this paper, the novel INDI technique is improved in theory, and implemented in real-world for the inner-loop force controller of the long-stroke hydraulic hexapod motion system of the SIMONA Research Simulator (SRS) at TU Delft. The key practical issues for INDI, such as additional dynamics between controller output and actuator sensor (including the valve dynamics and oil pipeline dynamics), are considered and solved. Directly combined with a typical computed force outer-loop controller with PD feedback in the actuator space, the overall motion control system is designed. Two motion profiles are used for experiments in this paper: a symmetric motion for control performance evaluation and benchmarking and an asymmetrical profile to validate the effectiveness of the proposed controller with more system nonlinearities excited.

The main contributions of this paper are: 1) The robustness of INDI against parameter uncertainty of the complete model, including the control related term, is rigorously proven for the first time, based on which a necessary stability condition for the INDI with parameter uncertainty is provided. A rigorous stability proof of the INDI is also given; 2) The novel INDI method is applied in a real-life hydraulic parallel robot for the first time; 3) The experiment results demonstrate improved control performance compared with the state-of-the-art methods discussed in a recent survey paper [24], even in existence of large model parameter mismatches.

This paper is organized as follows. Section II summarizes the model of the hydraulic robots for purpose of controller design. Section III introduces the novel INDI methodology, including the stability and robustness proofs. Section IV discusses the application details and practical issues in designing the INDI hydraulic control system. The experiment results on the SRS are described in Section V and the main conclusions are given in Section VI.

II. System Dynamic Model

The rigid-body dynamic equations of an n-link robot are generally given by a second-order nonlinear differential equation [23]. Particularly, for parallel robots such as hexapod robotic systems considered in this research as an example, Newton-Euler approach [30] is typically used to obtain the dynamic equations in Cartesian space:

$$\boldsymbol{M}(\boldsymbol{z})\,\ddot{\boldsymbol{s}} + \boldsymbol{\eta}(\dot{\boldsymbol{s}}, \boldsymbol{z}) = \boldsymbol{J}^T \boldsymbol{F}, \tag{1}$$

where $\boldsymbol{z} \in \mathbb{R}^6$ and $\dot{\boldsymbol{s}} \in \mathbb{R}^6$ are the end effector pose and velocity vectors defined in the Cartesian space, $\boldsymbol{F} \in \mathbb{R}^6$ is the vector of actuation forces, $\boldsymbol{M} \in \mathbb{R}^{6\times 6}$ is the mass matrix and $\boldsymbol{\eta} \in \mathbb{R}^6$ contains the centrifugal and Coriolis terms. $\boldsymbol{J} \in \mathbb{R}^{6\times 6}$ is the Jacobian matrix of the system, defined by $\boldsymbol{J} = \partial \dot{\boldsymbol{q}} / \partial \dot{\boldsymbol{s}}$, where $\boldsymbol{q}$ is the vector of the actuator displacements. A detailed discussion of the model can be found in [31].

A single symmetrical hydraulic actuator controlled by a typical valve is illustrated schematically in Fig. 2. Φ_{p1} and Φ_{p2} are the oil flows into and out of the cylinder chambers through the oil transmission lines. The oil supply and return pressures are denoted by P_s and P_t, respectively. The hydraulic force dynamics are generally described by writing the dynamic equation of the cylinder pressure difference, $P_L = P_{p1} - P_{p2}$, based on the oil compressibility effect, given by [29]:

$$\dot{P}_L = 2C_m(q)\left(\Phi_m - C_l P_L - A_p \dot{q}\right), \tag{2}$$

where q denotes the actuator cylinder displacement, A_p is the cylinder area, C_l is the leakage coefficient, $\Phi_m = (\Phi_{p1} + \Phi_{p2})/2$ is the controlled oil flow. The piston dependent oil stiffness C_m is

$$C_m = \frac{1}{2}\left(\frac{E}{V_1(q)} + \frac{E}{V_2(q)}\right), \tag{3}$$

where E is the oil bulk modulus and V_1 and V_2 are the volumes of the cylinder chambers.

For an ideal critical center valve with matched and symmetrical orifices, the oil flow is given by [32]

$$\Phi_m = C_d w x_m \sqrt{\frac{P_s}{\rho}\left(1 - \frac{x_m}{|x_m|}\frac{P_L}{P_s}\right)}. \tag{4}$$

where x_m is the valve displacement, C_d is the discharge coefficient and w is the orifice width.

By defining the maximum flow at the maximum valve stroke $x_{m,max}$ and zero load pressure as $\Phi_n = C_d w x_{m,max}\sqrt{P_s/\rho}$, and the system input as the normalized valve displacement $u = x_m/x_{m,max}$, (4) is substituted in (2) and gives:

$$\begin{aligned}\dot{P}_L &= 2C_m(q)\left(\Phi_n\sqrt{1 - \frac{x_m}{|x_m|}\frac{P_L}{P_s}}u - C_l P_L - A_p\dot{q}\right) \\ &= G_A(P_L, x_m, q)\,u + f_A(P_L, q, \dot{q}).\end{aligned} \tag{5}$$

The servo-valve dynamics are generally modeled as a second-order linear system with a bandwidth much higher than the rest of the system [3]. It will be shown in Section IV that with a valve displacement feedback in the proposed control scheme, the explicit use of the valve dynamic model can be avoided. The influence of the oil transmission line dynamics is also discussed in Section IV.

Combining (1) and (5) through the relation $F = A_p P_L$, the overall dynamic model of a hydraulic robot is given. Note that good lubrication is assumed for the hydraulic actuator and that frictions are considered as small continuous disturbances. Hence, friction is neglected for controller design, due to their smallness and the fact that the proposed INDI controller is inherently resistant to continuous disturbances, which will be discussed in Section III.

III. Incremental Nonlinear Dynamic Inversion

Traditional Nonlinear Dynamic Inversion (NDI) control is a variant of the feedback linearization [33] approach, which is widely used in flight control problems [34]. Similar approaches using inverse dynamics, such as computed torque [35] or flatness-based control [17], are also developed for other applications. However, a common disadvantage of feedback linearization based approaches is the dependency on a precise model and hence an inherent sensitivity to model uncertainties. The INDI technique implements the NDI method based on an incremental form of the system dynamics, in which the contribution of most model parameter dependent terms is minimized to a small perturbation. As a consequence, the INDI approach does not explicitly depend on precise model and is thus not sensitive to uncertainties.

A. Theory and Stability

The system of interest is a general n^{th} order nonlinear control inputs affine system given by

$$\begin{aligned}\dot{\boldsymbol{x}} &= \boldsymbol{f}(\boldsymbol{x}) + \boldsymbol{G}(\boldsymbol{x})\,\boldsymbol{u} + \boldsymbol{d} \\ \boldsymbol{y} &= \boldsymbol{h}(\boldsymbol{x}),\end{aligned} \tag{6}$$

where $\boldsymbol{f}$ is a vector field in $\mathbb{R}^n$, $\boldsymbol{u} \in \mathbb{R}^m$ is the input, $\boldsymbol{d} \in \mathbb{R}^n$ is a continuous external disturbance and $\boldsymbol{G} \in \mathbb{R}^{n\times m}$ is the control effectiveness matrix. $\boldsymbol{x}$, $\boldsymbol{d}$ and $\boldsymbol{h}$ are assumed continuous, $\boldsymbol{f}(\boldsymbol{x})$ and $\boldsymbol{G}(\boldsymbol{x})$ are assumed to be $\mathcal{C}^\infty$ functions of $\boldsymbol{x}$ and all degrees of differentiation are bounded.

Assuming that $\boldsymbol{h}(\boldsymbol{x}) = \boldsymbol{x}$, the relative degree of the system is $(1, \cdots, 1)_{1\times n}$, and the first-order time derivative of the output is

$$\dot{\boldsymbol{y}} = \dot{\boldsymbol{x}} = \boldsymbol{f}(\boldsymbol{x}) + \boldsymbol{G}(\boldsymbol{x})\,\boldsymbol{u} + \boldsymbol{d}, \tag{7}$$

where the control input $\boldsymbol{u}$ appears explicitly in the above equation. For a fully actuated system for which $m = n$, the traditional NDI, or a general feedback linearization approach, can be implemented if $\boldsymbol{G}(\boldsymbol{x})$ is invertible.

Different from the NDI approach, in order to obtain the incremental form of the studied system, the system dynamics in (7) are rewritten by applying the Taylor series expansion at the beginning instant of each sampling interval (denoted by subscript 0):

$$\begin{aligned}\dot{\boldsymbol{x}} = \dot{\boldsymbol{x}}_0 + \boldsymbol{G}(\boldsymbol{x}_0)(\boldsymbol{u} - \boldsymbol{u}_0) + \left.\frac{\partial[\boldsymbol{f}(\boldsymbol{x}) + \boldsymbol{G}(\boldsymbol{x})\,\boldsymbol{u}]}{\partial \boldsymbol{x}}\right|_0 (\boldsymbol{x} - \boldsymbol{x}_0) \\ + (\boldsymbol{d} - \boldsymbol{d}_0) + \boldsymbol{O}\left((\boldsymbol{x} - \boldsymbol{x}_0)^2\right).\end{aligned} \tag{8}$$

Defining the last three terms of (8) as

$$\boldsymbol{\delta}(\Delta\boldsymbol{x}, \Delta\boldsymbol{d}) = \left.\frac{\partial[\boldsymbol{f}(\boldsymbol{x}) + \boldsymbol{G}(\boldsymbol{x})\,\boldsymbol{u}]}{\partial \boldsymbol{x}}\right|_0 \Delta\boldsymbol{x} + \Delta\boldsymbol{d} + \boldsymbol{O}\left(\Delta\boldsymbol{x}^2\right), \tag{9}$$

in which the increments of the variables with respect to their current values are denoted by Δ, (8) is then written as

$$\dot{\boldsymbol{x}} = \underbrace{\dot{\boldsymbol{x}}_0 + \boldsymbol{G}(\boldsymbol{x}_0)(\boldsymbol{u} - \boldsymbol{u}_0)}_{\text{nominal part}} + \underbrace{\boldsymbol{\delta}(\Delta\boldsymbol{x}, \Delta\boldsymbol{d})}_{\text{perturbation}}, \tag{10}$$

In (10) the system dynamics are divided into an incremental nominal part, which contains the first two terms, and a perturbation term.

Using the continuity of $\boldsymbol{x}$ and $\boldsymbol{d}$ and the boundedness of the differentiation of $\boldsymbol{f}(\boldsymbol{x})$ and $\boldsymbol{G}(\boldsymbol{x})$, the limits of (9) as the time increment T_s goes to 0 is calculated as

$$\lim_{T_s \to 0} \boldsymbol{\delta}(\Delta\boldsymbol{x}, \Delta\boldsymbol{d}) = 0. \tag{11}$$

(11) suggests that with a fast sampling rate, the contribution of the perturbation $\boldsymbol{\delta}$ to the system dynamics in (10) approaches zero. Note that the continuity is not assumed for the system input $\boldsymbol{u}$ in (10). Thus the INDI control law is designed by using the NDI based on the nominal part of (10) *in every sampling interval*, given by

$$\boldsymbol{u} = \boldsymbol{u}_0 + \boldsymbol{G}^{-1}(\boldsymbol{x}_0)(\boldsymbol{\nu} - \dot{\boldsymbol{x}}_0), \tag{12}$$

where $\boldsymbol{\nu}$ is the pseudo control input to be determined and the system state derivatives $\dot{\boldsymbol{x}}_0$ are assumed to be measured. Note that the subscript 0 means the beginning of every sampling interval, instead of a fixed reference point. For every sampling interval, the control increment $\Delta\boldsymbol{u} = \boldsymbol{G}^{-1}(\boldsymbol{x}_0)(\boldsymbol{\nu} - \dot{\boldsymbol{x}}_0)$ is calculated and recursively added to $\boldsymbol{u}_0$, the integrated or measured control input of the previous sample, as illustrated in the block diagram presented in Fig. 3. Thus the control law (12) can also be written in a recursive discrete form as:

$$\begin{aligned}\boldsymbol{u}_k &= \boldsymbol{u}_{k-1} + \Delta\boldsymbol{u} \\ \Delta\boldsymbol{u} &= \boldsymbol{G}^{-1}(\boldsymbol{x}_{k-1})(\boldsymbol{\nu} - \dot{\boldsymbol{x}}_{k-1}),\end{aligned} \tag{13}$$

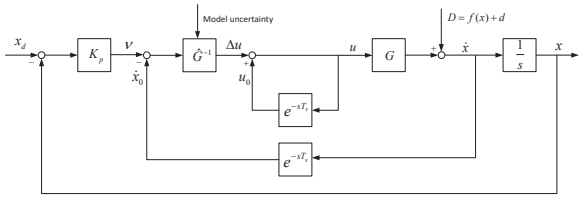

Fig. 3. Block diagram of a general INDI controller

Substituting (12) into (10), the closed-loop system dynamics are given by

$$\dot{\boldsymbol{x}} = \boldsymbol{\nu} + \boldsymbol{\delta}\left(\Delta\boldsymbol{x}, \Delta\boldsymbol{d}\right). \tag{14}$$

Combining (11) and (14), it is clear that under an infinitesimal sampling time, the system is fully linearized. By simply choosing the linear control law $\boldsymbol{\nu} = \dot{\boldsymbol{x}}_d + K_p\left(\boldsymbol{x}_d - \boldsymbol{x}\right)$, where $-K_p$ is Hurwitz and the subscript d denotes the desired trajectory, the system error dynamics are written as

$$\dot{\boldsymbol{e}} = -K_p\boldsymbol{e} + \boldsymbol{\delta}\left(\Delta\boldsymbol{x}, \Delta\boldsymbol{d}\right), \tag{15}$$

where $\boldsymbol{e} = \boldsymbol{x} - \boldsymbol{x}_d$. With an infinitesimal T_s, the origin of (15) is globally exponentially stable. This is the reason that the INDI is based on the assumption of a high sampling rate. However, in practice, the small sample time T_s is a finite value. (11) suggests that $\forall\, \varepsilon > 0$, $\exists\, T_s > 0$, s.t. $\|\boldsymbol{\delta}\left(\Delta\boldsymbol{x}, \Delta\boldsymbol{d}\right)\|_2 \leq \varepsilon$. Thus the stability of INDI is given by the lemma below.

Lemma 1: Consider the closed-loop system in (15), where $-K_p$ is Hurwitz, if $\|\boldsymbol{\delta}\left(\Delta\boldsymbol{x}, \Delta\boldsymbol{d}\right)\|_2 \leq \varepsilon$, the error $\boldsymbol{e}$ will be globally ultimately bounded by εc for some $c > 0$.

Proof: applying Lemma 13.4 in [36]. □

Lemma 1 shows that the tracking error of the proposed INDI controlled system is globally ultimately bounded and that the ultimate bound can be decreased by reducing the magnitude of the perturbation term $\boldsymbol{\delta}\left(\Delta\boldsymbol{x}, \Delta\boldsymbol{d}\right)$ in a single time increment, with a higher controller sampling frequency. In practice, the perturbation term is sufficiently small with a sufficiently high sampling frequency such that it can be neglected from (14). Besides, a simple proportional controller is generally chosen for the pseudo control $\boldsymbol{\nu}$, as the system is linearized as a single integrator. Fig. 3 gives the general structure of the INDI controller, where e^{-sT_s} denotes the transport delay in a single sample time T_s. When model uncertainties exist for $\boldsymbol{G}$, the estimated value $\widehat{\boldsymbol{G}}$ is used for the controller.

Note that in the INDI control law (12), the information of $\dot{\boldsymbol{x}}_0$ is assumed to be obtained by reliable sensor measurements and updated in every sampling period. Consider the system dynamics in (10), by reducing the sampling time, the contribution of the perturbation term to the system dynamics is reduced to be significantly less than the rest nominal part that contains $\dot{\boldsymbol{x}}_0$. Thus INDI is dependent on its accurate measurement.

B. Robustness to Parameter Uncertainty and Disturbance

Considering the general system given by (6), INDI is inherently insensitive to parameter uncertainty in $\boldsymbol{f}\left(\boldsymbol{x}\right)$ and continuous disturbances $\boldsymbol{d}$. This is because information of these quantities is not explicitly used in the INDI control law in (12), and the contribution of these two terms to the system dynamics only appear in the perturbation term which, will only influence the ultimate bound of the error dynamics and can be reduced to be negligible by increasing the sampling rate.

It is observed in various applications that INDI is also insensitive to parameter uncertainty in the matrix $\boldsymbol{G}\left(\boldsymbol{x}\right)$ in (6), with according proofs [25], [26]. However, all these proofs are based on the assumption that $\dot{\boldsymbol{x}} = \dot{\boldsymbol{x}}_0$ with small time increment. This assumption requires the continuity of $\dot{\boldsymbol{x}}$, which conflicts with the basic assumption of the INDI that the system input $\boldsymbol{u}$, and consequently the state derivative $\dot{\boldsymbol{x}}$, are not necessarily continuous. This was also pointed out in [37], in which, however, a new proof was not given. In this section, it is rigorously proven that INDI is insensitive to parameter uncertainty in $\boldsymbol{G}\left(\boldsymbol{x}\right)$ without requiring the continuity of $\dot{\boldsymbol{x}}$.

First consider a SISO system for which $\boldsymbol{G}$ is a scalar. In Fig. 3, with the assumption of high sampling rate, the system dynamics of $\boldsymbol{G}$ is regarded as a slowly varying gain of a input-linear system. $\boldsymbol{f}\left(\boldsymbol{x}\right) + \boldsymbol{d}$ is regarded as a lumped disturbance term, i.e., $\boldsymbol{D} = \boldsymbol{f}\left(\boldsymbol{x}\right) + \boldsymbol{d}$, the increment of which in one sampling period is $\boldsymbol{\delta}$ in (11). When the estimated $\widehat{\boldsymbol{G}}$ is used for the controller, the transfer function from $\boldsymbol{\nu}\left(s\right)$ to $\dot{\boldsymbol{x}}\left(s\right)$ can be easily calculated as

$$\begin{aligned} H\left(s\right) = \frac{\dot{\boldsymbol{x}}\left(s\right)}{\boldsymbol{\nu}\left(s\right)} &= \frac{\boldsymbol{G}\widehat{\boldsymbol{G}}^{-1}}{1 + \left(\boldsymbol{G}\widehat{\boldsymbol{G}}^{-1} - 1\right)e^{-sT_s}} \\ &= \frac{1}{\alpha + \left(1 - \alpha\right)e^{-sT_s}}, \end{aligned} \tag{16}$$

where $\alpha = \widehat{\boldsymbol{G}}\boldsymbol{G}^{-1}$ indicates the level of model mismatch.

Replacing e^{-sT_s} in (16) by z^{-1}, the stability condition of the equivalent z-domain transfer function is that the poles are located inside the unit circle, which requires that $\alpha > 0.5$. Considering the frequency response of $H\left(j\omega\right)$, it can be proven that if $\alpha > 0.5$, the real part of $H\left(j\omega\right)$ is always positive for any ω, and thus the phase angle of $H\left(j\omega\right)$ satisfies

$$-0.5\pi < \angle H\left(j\omega\right) < 0.5\pi, \text{ if } \alpha > 0.5. \tag{17}$$

According to the final value theorem, the step response of $H\left(s\right)$ is $\lim_{s\to\infty} H\left(s\right) = 1$. This means that if only the estimated $\widehat{\boldsymbol{G}}$ is bigger than half of the real $\boldsymbol{G}$ ($\alpha > 0.5$), $\dot{\boldsymbol{x}}$ will converge to $\boldsymbol{\nu}$. Thus the model uncertainty in $\widehat{\boldsymbol{G}}$ introduces dynamics, instead of a disturbance, to the linearized single integrator $\boldsymbol{\nu} = \dot{\boldsymbol{x}}$. The speed of the dynamics would increase when the sample time T_s decreases. In fact, (16) shows that $H\left(s\right)$ is equal to 1 when T_s approaches zero. This proves why the INDI controller is robust to model uncertainty in $\boldsymbol{G}$.

The robustness of INDI against uncertainty in $\boldsymbol{f}\left(\boldsymbol{x}\right)$ and $\boldsymbol{d}$ has been explained in the time domain, but can be further verified by calculating the closed-loop transfer function from the lumped disturbance $\boldsymbol{D} = \boldsymbol{f}\left(\boldsymbol{x}\right) + \boldsymbol{d}$ to $\dot{\boldsymbol{x}}$, which is

$$\frac{\dot{\boldsymbol{x}}\left(s\right)}{\boldsymbol{D}\left(s\right)} = \frac{1 - e^{-sT_s}}{1 - e^{-sT_s} + \boldsymbol{G}\widehat{\boldsymbol{G}}^{-1}e^{-sT_s}}. \tag{18}$$

When the controller sampling rate is sufficiently high, the magnitude of (18) approaches 0 as T_s approaches 0. This is consistent with the fact that $\boldsymbol{\delta}$ becomes negligible when T_s is

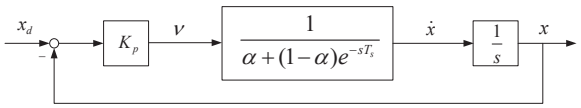

Fig. 4. The transfer function of the controlled system

small. Besides, even without this assumption, according to the final value theorem, the step response of (18) converges to 0. This means that the lumped disturbance term $\boldsymbol{D} = \boldsymbol{f}(\boldsymbol{x}) + \boldsymbol{d}$ is inherently rejected over time, and its influence is further attenuated with a small sampling period.

The transfer function of the controlled system is thus given in Fig. 4. The open-loop transfer function is

$$P(s) = \frac{K_p}{s\left(\alpha + (1-\alpha)\, e^{-sT_s}\right)} = \frac{K_p}{s} H(s). \tag{19}$$

According to (16) and (17), if $\alpha > 0.5$, $P(s)$ is stable and its phase angle satisfies $-\pi < \angle P(j\omega) < 0$ because $\angle P(j\omega) = -0.5\pi + \angle H(j\omega)$. This means the Nyquist plot of $\angle P(j\omega)$ will stay below (and will never intersect) the real axis. This first means that the open-loop Nyquist plot will never encircle the -1+i0 point, which guarantees the stability of the closed-loop system. Second, as the Nyquist plot of $\angle P(j\omega)$ will always intersect with the unit circle below the real axis, the controlled system always has positive phase margin and infinite gain margin in the presence of model uncertainty. Note that the validity of (16) to (19) relies on the linearization of the system within a single sampling period in (10), which requires a fast sampling rate.

This proves the robustness of INDI for SISO systems with a single necessary condition $\widehat{\boldsymbol{G}}\boldsymbol{G}^{-1} > 0.5$, which will be validated with experiments in Section V. It can be extended to MIMO systems with the following lemma.

Lemma 2: If the square matrix $\widehat{\boldsymbol{G}}\boldsymbol{G}^{-1}$ is diagonalizable and all its eigenvalues are real and bigger than 0.5, then the nominal part of (10) can still be exactly linearised to be $\dot{\boldsymbol{x}} = \boldsymbol{\nu}$, given the control law in (12) with estimated control effectiveness matrix $\widehat{\boldsymbol{G}}$, with an infinitesimal sample time T_s.

Proof: The INDI control law with parameter uncertainty in $\widehat{\boldsymbol{G}}(\boldsymbol{x})$ is given by

$$\boldsymbol{u} = \boldsymbol{u}_0 + \widehat{\boldsymbol{G}}^{-1}(\boldsymbol{x}_0)\left(\boldsymbol{\nu} - \dot{\boldsymbol{x}}_0\right), \tag{20}$$

thus the nominal dynamics of (10) become

$$\dot{\boldsymbol{x}} = \dot{\boldsymbol{x}}_0 + \boldsymbol{G}\widehat{\boldsymbol{G}}^{-1}\left(\boldsymbol{\nu} - \dot{\boldsymbol{x}}_0\right). \tag{21}$$

Considering (21) as a linear system with slowly changing gain $\boldsymbol{G}\widehat{\boldsymbol{G}}^{-1}$ (as the sampling rate is high), and describing it in terms of samples instead of signals, we obtain

$$\dot{\boldsymbol{x}}_{(k)} = \dot{\boldsymbol{x}}_{(k-1)} + \boldsymbol{G}\widehat{\boldsymbol{G}}^{-1}\left(\boldsymbol{\nu}_{(k)} - \dot{\boldsymbol{x}}_{(k-1)}\right), \tag{22}$$

which is identical to

$$\widehat{\boldsymbol{G}}\boldsymbol{G}^{-1}\dot{\boldsymbol{x}}_{(k)} = \left(\widehat{\boldsymbol{G}}\boldsymbol{G}^{-1} - I\right)\dot{\boldsymbol{x}}_{(k-1)} + \boldsymbol{\nu}_{(k)}. \tag{23}$$

Consider the eigenvalue decomposition of the matrix $\widehat{\boldsymbol{G}}\boldsymbol{G}^{-1}$

$$\widehat{\boldsymbol{G}}\boldsymbol{G}^{-1} = \boldsymbol{M}\boldsymbol{\Lambda}\boldsymbol{M}^{-1}, \tag{24}$$

and the state variable transformation

$$\dot{\boldsymbol{\chi}} = \boldsymbol{M}^{-1}\dot{\boldsymbol{x}},\ \boldsymbol{\upsilon} = \boldsymbol{M}^{-1}\boldsymbol{\nu}, \tag{25}$$

then (23) is transformed to diagonal form:

$$\boldsymbol{\Lambda}\dot{\boldsymbol{\chi}}_{(k)} = (\boldsymbol{\Lambda} - I)\,\dot{\boldsymbol{\chi}}_{(k-1)} + \boldsymbol{\upsilon}_{(k)}, \tag{26}$$

the system is transformed into n decoupled scalar equations:

$$\lambda_i \dot{\chi}_{i(k)} = (\lambda_i - 1)\,\dot{\chi}_{i(k-1)} + \upsilon_{i(k)}. \tag{27}$$

Taking the z-transform to the above equations, the transfer function between the transformed pseudo control inputs and system state derivatives is calculated as:

$$H_i(z) = \frac{\dot{\boldsymbol{\chi}}_i(z)}{\boldsymbol{\upsilon}_i(z)} = \frac{1}{\lambda_i + (1-\lambda_i)\, z^{-1}}, \tag{28}$$

which turns out to be a discrete filter that has a stable pole inside the unit circle when $\lambda_i > 0.5$. When the sample time T_s is infinitesimal, the normalized frequency $\omega = fT_s$ approaches zero, thus the frequency response of $H_i(z)$ is

$$\lim_{T_s \to 0} H_i\left(e^{jfT_s}\right) = \frac{1}{\lambda_i + (1-\lambda_i)} = 1, \tag{29}$$

Combining this result with (25), we obtain $\dot{\boldsymbol{x}} = \boldsymbol{\nu}$. □

Lemma 2 shows that (14) still holds with parameter uncertainty in $\boldsymbol{G}(\boldsymbol{x})$ for a high sampling rate. The uncertainty adds dynamics in the form of a stable discrete filter in (28) for the linearized nominal system, instead of disabling it as in the case of traditional feedback linearization.

In practice the controller sampling rate for INDI is chosen to be sufficiently higher than that of the trajectory signal, which validates the assumption of a infinitesimal normalized frequency. Lemma 2 also gives the tolerance of the INDI to the model mismatch of $\boldsymbol{G}(\boldsymbol{x})$, as a condition for (28) to be stable.

In conclusion, INDI is a practical nonlinear control technique for overcoming the sensitivity to parameter uncertainties and continuous disturbances of traditional feedback linearization methods.

The proposed INDI controller is similar in form to the well-known Time-Delay-Control (TDC) technique [38], which also introduced an incremental form of the control law. However, both have totally different theoretical bases. Consequently, different approaches are used to prove stability and robustness. Besides these differences, the application of this incremental form of control law on hydraulic force control problems has so far not been reported.

IV. Controller Design

This section addresses the design of the INDI-based hydraulic actuator force controller for the SRS, a 6-DOF hydraulic parallel robot, which is illustrated in Fig. 5. Implementation issues such as valve dynamics and oil pipeline dynamics are discussed. As a baseline controller to be compared with, a traditional NDI-based force controller is briefly introduced. A force computation outer-loop motion controller is combined with the proposed inner-loop controller to close the loop of the complete motion control system, as proposed in Fig. 1. Note that the proposed approach can be applied to more general outer-loop controllers.

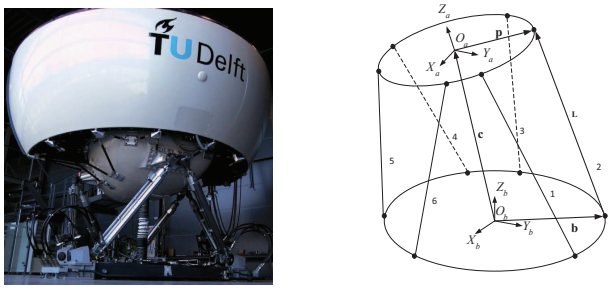

Fig. 5. A hexapod motion system SRS at TU Delft (left), and a its schematic drawing (right) [29]

A. Inner-loop INDI hydraulic force controller

The hydraulic actuator dynamics given by (5) are a first-order system with a relative degree of 1 if we choose the state P_L as the output. The control effectiveness matrix $\boldsymbol{G}$ is G_A in this case, which is a scalar and it is not equal to zero except in the case of load saturation. In practice, a small constant is chosen for G_A in the controller when it is smaller than a particular value, in order to avoid singularity. By choosing a high-bandwidth servo-valve, the valve dynamics bandwidth is well above that of the rest of the system (the bandwidth of the servo-valve is around $150Hz$ for the SRS) [39]. As pressure sensors are commonly used in the hydraulic actuators, the state measurement is generally available. Thus, all assumptions and conditions for INDI are fulfilled for the studied hydraulic system.

Consider the hydraulic pressure dynamics in (5), the actuator velocity term $2C_m A_p \dot{q}$ exists as an interaction from the platform dynamics. It is considered as a continuous disturbance to the local pressure dynamics. Following the procedure of the INDI methodology from (8) to (14), the incremental form pressure dynamics are written as

$$\dot{P}_L = \dot{P}_{L0} + G_A \left(u - u_0\right) + \delta \left(\Delta \dot{q}, \Delta P_s\right), \tag{30}$$

where

$$G_A = 2C_m \left(q_0\right) \Phi_n \sqrt{1 - sgn\left(x_{m0}\right) \frac{P_{L0}}{P_s}}. \tag{31}$$

Linearizing the nominal part of (30), the INDI control law is given by [29]

$$u = u_0 + G_A^{-1} \left(\nu - \dot{P}_{L0}\right), \tag{32}$$

and the linear relation between ν and $\dot{P}_L$ is achieved in existence of the perturbation term:

$$\dot{P}_L = \nu + \delta \left(\Delta \dot{q}, \Delta P_s\right). \tag{33}$$

By choosing a sufficiently high controller sampling rate, the magnitude of the perturbation is reduced to be negligible. A simple linear controller can be chosen for ν, turning the hydraulic system into a force generator:

$$\dot{P}_L = \nu = K_p \left(F_{ref}/A_p - P_L\right), \tag{34}$$

where F_{ref} is the desired actuation force.

From a controller design perspective, the INDI approach is straightforwardly implementable for control applications in industry, and the stability and robustness against uncertainties are guaranteed by Lemma 1 and Lemma 2. The effectiveness of the proposed controller is verified in simulation work in [29]. However, some implementation issues are met in real-world application for the SRS. It will be shown below that they can be solved with simple techniques integrated in the framework of the INDI method.

B. Solving implementation issues

1) Numerical differentiation: The derivative of the current actuator pressure difference $\dot{P}_{L0}$ is required by the INDI control law in (32), which is typically not directly available as measurement. In practice it is obtained by numerical differentiation of the measurement of the pressure sensor available on most hydraulic actuators. The noises amplified by numerical differentiation are attenuated by a typical low-pass filter [27]. As will be discussed in Section IV-B3, the filter also has another purpose, that is, to attenuate the oil pipeline dynamics, thus the corresponding solution for the common issue of the introduced phase lag will be discussed in detail there.

In addition to the practical low-pass filter, more advanced differentiation methods such as Kalman filters or Savitzky-Golay filters [40] can be considered to deal with the noise. Note, however, that for applications to other systems, the state derivatives may be directly measured. For instance, the angular acceleration of an aircraft or robotic systems can be measured with angular accelerometers.

2) Valve dynamics: The theoretical INDI control law given by (32) is in the form of the accumulation of the control increments calculated in each time step. This requires the assumption of infinitely fast actuator dynamics, which in the hydraulic system applies to the servo-valve dynamics. In practice, the finite actuator bandwidth may cause stability problems [27], even if it is sufficiently higher than that of the rest of the system. Thus in real-world applications, the real-time measurement of the hydraulic servo-valve spool position is used for u_0 in (32) (as shown in Fig. 8), instead of the theoretical memory of the accumulated control input. It will be shown in (35) that by doing this, with stable servo-valve dynamics, the system stability will not be influenced.

3) Transmission line dynamics: For hydraulic applications such as flight simulators, the relatively large operational space asks for long-stroke actuators, which inherently introduce high-frequency transmission dynamics of the relatively long oil pipelines between the valve and the actuator, as shown in Fig. 2. The modeling of these transmission dynamics was extensively studied in literature [41]. In [42], the so-called "model approximation technique" is adopted to describe the transmission dynamics by an infinite product series of second order models, each of which gives rise to a resonance mode. In the case of the SRS, with the pipelines of around 1.2 meters, a linearized model analysis shows resonance frequencies at 200, 600, 1000 Hz and higher [42]. Given a digital controller at 5000 Hz and valve bandwidth up to about 150 Hz, the first mode is relevant for controller design and analysis.

Fig. 6 shows the Bode plots from the input x_m to the output P_L of a hydraulic actuator model including the transmission

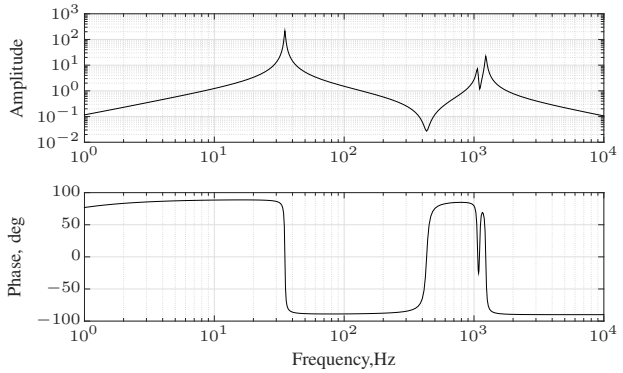

Fig. 6. Bode plot of hydraulically driven mechanical system model including transmission lines. Input valve displacement x_m, output hydraulic load pressure difference P_L

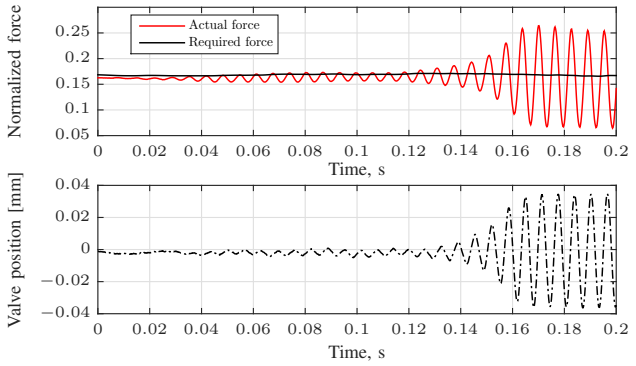

Fig. 7. High frequency oscillation of load pressure and valve due to the resonance frequencies of transmission lines.

lines. The eigenfrequencies of the two transmission lines at around 200 Hz combined with the 180° phase lag brought on by the valve dynamics cause stability problems by pressure feedback [39], [42]. In early experiments without consideration of these effects, a heavy self-sustaining oscillation at about 200 Hz occurred for the proposed controller, as shown in Fig. 7.

The easiest way to solve this problem is to add a second-order low-pass filter $H_t(z)$ in the pressure feedback loop before the differentiator (see Fig. 8), in order to attenuate the resonance peaks and shift the crossover frequency. In practice, a filter with a 35 Hz natural frequency is used for the SRS, with a balance of stability and performance based on trial and error experiments. As discussed before, $H_t(z)$ has a second purpose in smoothing the P_L measurement, thereby avoiding the amplification of the measurement noise by the numerical differentiation.

As a result, the filtered pressure measurement $\dot{P}_{Lf}$, instead of the real value $\dot{P}_{L0}$, is used for feedback. Extra dynamics are thus introduced to the loop and the phase lag introduced by $H_t(z)$ will degrade the control performance [25]. In this study, the technique proposed in literature [27] is adopted, where $H_t(z)$ is also added in the valve spool position measurement loop, as shown in Fig. 8. It will be shown in (35) that with this compensation, the influence of the additional dynamics is canceled from the system dynamics. We emphasize here that

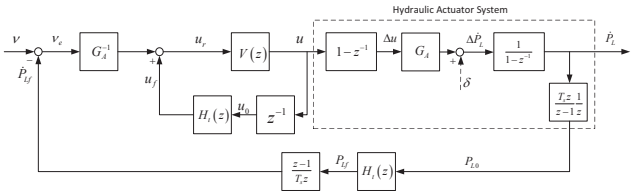

Fig. 8. Practical INDI control scheme for inner-loop hydraulic actuator force tracking.

the synchronization of the filters in both loops is an important practical solution for dealing with the phase lag introduced by state derivative estimation.

Taking these issues into consideration, the INDI force controller implemented in reality is illustrated in Fig. 8 with a z-domain block diagram representation, where $V(z)$ denotes the valve dynamics and the subscript f denotes the filtered signals. The system dynamics in the dotted line box is based on the incremental form of system dynamics given in (30). The controller follows the framework proposed in previous theoretical work [29].

The strategies introduced in this section can be easily verified by calculating the closed-loop transfer function from ν to $\dot{P}_L$:

$$\begin{aligned}\frac{\dot{P}_L(z)}{\nu(z)} &= \frac{V(z)\left(1-V(z)H_t(z)z^{-1}\right)^{-1}}{1+V(z)\left(1-V(z)H_t(z)z^{-1}\right)^{-1}H_t(z)z^{-1}} \\ &= \frac{V(z)}{1-V(z)H_t(z)z^{-1}+V(z)H_t(z)z^{-1}} = V(z).\end{aligned} \tag{35}$$

The valve dynamics $V(z)$ show up in the controlled system transfer function, instead of a single integrator in (34). (35) suggests that by using the servo-valve output measurement as feedback, system stability is not influenced with the stable servo-valve dynamics. With this measurement, the valve dynamics are considered in the control system, while a precise model is not necessary. It is also verified that the introduction of the filter $H_t(z)$ in the control input memory loop canceled its influence on the measurement feedback loop. With this simple relation, the proportional controller of (34) is still sufficient to stabilize the system. The use of input measurement feedback and the compensation filter in that loop to deal with unmodeled dynamics are the main features of the practical INDI technique.

C. Inner-loop NDI based force controller

NDI is a more traditional nonlinear control strategy as an example of feedback linearization. A direct application can be made to the hydraulic pressure dynamic equation given in (5) by simply inverting it as follows:

$$u = G_A^{-1}(P_L, x_m, q)\left(\nu - f_A(P_L, q, \dot{q})\right), \tag{36}$$

and the pressure dynamics become $\dot{P}_L = \nu$, which allows for a simple linear controller for ν. This strategy is adopted in various applications [3], [43]. Variants of NDI are also called "cascade ΔP" (CdP) or "cascade" control for some hydraulic

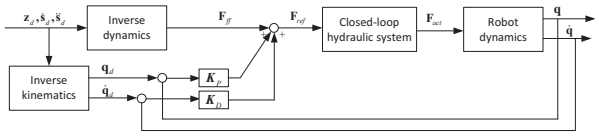

Fig. 9. Outer-loop computed torque controller with PD feedback for the SRS

control applications [16], [44], [45], which have also been adopted for the SRS [39]. Such NDI-based controllers rely on an accurate model and it will be shown that the performance is significantly degraded when parameter mismatches exist.

D. Outer-loop motion controller

As in this study we focus on the novelty of the inner-loop INDI force controller, a widely applied computed torque control approach [6] is used for the outer-loop controller, as illustrated by Fig. 9. A feedforward force $\boldsymbol{F}_{ff}$ is calculated by the inverse dynamics of the hexapod and added to the PD feedback terms in the actuation space, before it is sent to the closed-loop hydraulic subsystem. The outer-loop control law is given by:

$$\boldsymbol{F}_{ref} = \boldsymbol{F}_{ff} + \boldsymbol{K}_P \left(\boldsymbol{q}_d - \boldsymbol{q}\right) + \boldsymbol{K}_D \left(\dot{\boldsymbol{q}}_d - \dot{\boldsymbol{q}}\right). \tag{37}$$

V. Experiment Results

This section demonstrates the force control performance of the proposed INDI technique for motion tracking tasks for the hydraulic hexapod motion system of the SRS at TU Delft, for both nominal conditions and cases with significant parameter mismatches. The overall system performance is also demonstrated and compared to a baseline NDI approach, as well as other similar state-of-the-art control schemes.

A. Hardware Setup

The SRS is a 6-DOF flight simulator with a movable mass of around 4000 kg, capable of carrying two pilots, as shown in Fig. 5. The SRS is equipped with a hexapod motion system consisting of six hydraulic cylinders with 1.25 meters total stroke. With a 160 bar working pressure, the actuators are capable of exerting a maximum force of $F_m = 40$ kN, with a 1 m/s maximum actuator velocity. Each actuator is equipped with a Rexroth 4WSE3EE three-stage servo-valve and a PAINE 210-60-090 pressure transducer. Temposonic position sensors are installed on the actuators for position measurement and velocity estimation. The nominal parameters for the actuator model were identified in off-line experiments for the NDI-based controller as a baseline.

The motion control computer (MCC) is equipped with the dSPACE DS1005 system clocked at 1 GHz. The inner-loop controller is sampled at 5000 Hz and the outer-loop controller at 1000 Hz. The filters are designed in the analog plane and discretized using the bilinear transformation.

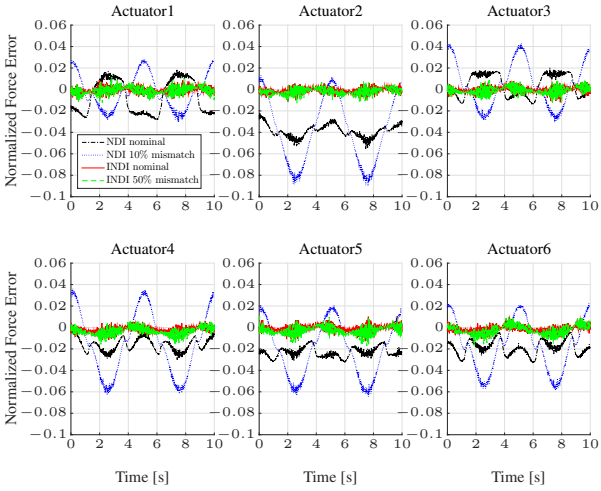

Fig. 10. Inner-loop force tracking errors for NDI and INDI in nominal and parameter mismatch conditions.

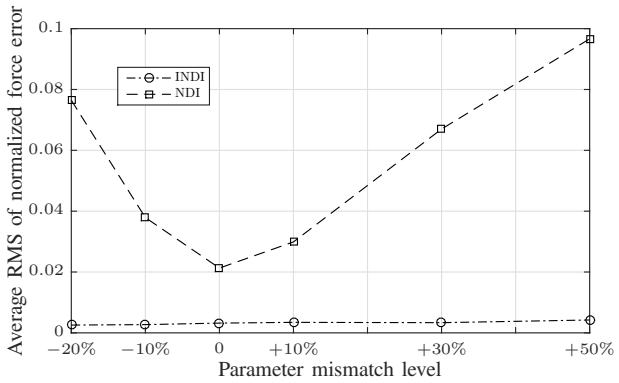

Fig. 11. Average RMS of nomalized force tracking errors of all actuators for the NDI and INDI controllers at different parameter mismatch levels.

B. Motion Profile 1

A set of symmetric motion tracking tasks along the vertical axis are tested first to demonstrate the efficiency of the proposed method with nominal hydraulic parameters. The force tracking error (normalized by $P_s A_p$) of each actuator with the INDI controller and the NDI-based controller in tracking the reference trajectory $z_d = 0.2 \sin 0.4\pi t$ m around the neutral point are shown in Fig. 10. The maximum tracking error is consistently around 1% for the INDI controller and $2.5\% - 4\%$ for the NDI controller. The performance of the INDI controller is consistently better than that of the NDI controller. The performance of NDI varies significantly for the different actuators, due to the different individual nonlinear dynamics that are not completely canceled. The advantage of INDI is thus already obvious in the nominal case.

The robustness of the INDI controller against parameter uncertainties is demonstrated by intentionally introducing parameter mismatches to the controller in the motion tracking test. In practice, the uncertainty of G_A results from model mismatches of Φ_n, C_m or disturbances of P_s. In this paper, the value of G_A used for the controller is offset from the nominal case, as would for instance be caused by the proportional mismatches

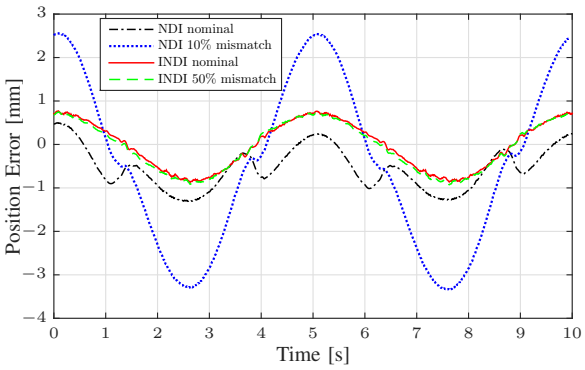

Fig. 12. Position tracking errors for NDI and INDI in nominal and offset conditions.

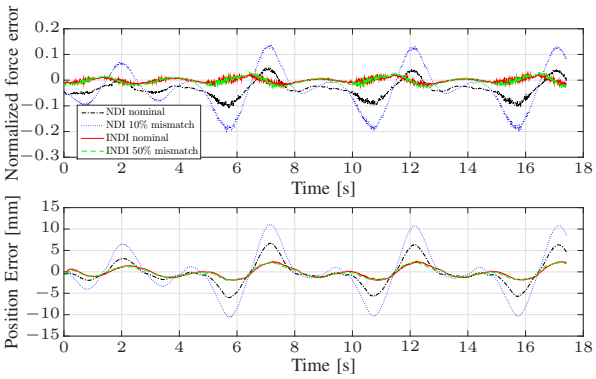

Fig. 13. Force and position tracking errors for NDI and INDI in nominal and parameter mismatch conditions for actuator 2 with the aggressive manoeuvre of motion profile 2.

TABLE I
ρ INDICATORS COMPARED WITH STATE-OF-THE-ART STUDIES

Study	ρ [s]	$\lvert e\rvert_{\max}$ [mm]	DOF	Type
Koivumaki 2015 [22]	0.0050	5.20	3	serial
Sirouspour 2001 [23]	0.0100	2.60	6	parallel
INDI nominal	0.0035	0.87	6	parallel
INDI 50% mismatch	0.0036	0.91	6	parallel

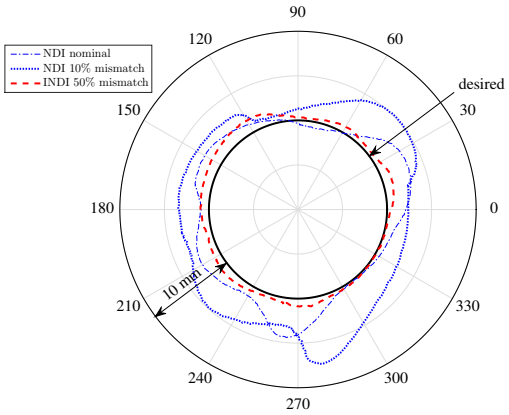

Fig. 14. Position tracking performance in horizontal plane for NDI and INDI in nominal and parameter mismatch conditions for motion profile 2.

of the maximum oil flow Φ_n, between their estimated and real values. The force tracking errors in mismatch conditions for INDI and NDI are also shown in Fig. 10. The performance of the NDI controller is significantly degraded with only +10% mismatch of $\widehat{G}_A$, while that of the INDI controller remains almost intact for up to 50% parameter mismatch. Fig. 11 gives the average Root-Mean-Square (RMS) of the nomalized force tracking error of all actuators for both controllers, under different levels of parameter mismatch in terms of $\widehat{G}_A$, from -20% to +50%. The INDI shows equivalent performance at each condition, with an RMS of around 0.003, while that of the NDI quickly deteriorates from 0.02 to 0.1 as the mismatch level increases.

This result validates that INDI is resistant to even an unrealistic magnitude of error in parameter estimation for G_A while keeping high-precision performance, as long as the necessary condition $\alpha = \widehat{G}_A G_A^{-1} > 0.5$ (see Section III) is fulfilled. Note that INDI is inherently not sensitive to the leakage term $C_l P_L$ and the velocity related term $A_p \dot{q}$ in (5), as they are minimized as the perturbation term and do not appear in the control law at all.

Combined with the same outer-loop controller, the overall position tracking errors of both controllers are shown in Fig. 12. The maximum position error of the NDI controller is 1.303 mm in nominal condition, and is rapidly increased to 3.3 mm with only +10% mismatch on $\widehat{G}_A$. The performance of INDI is insensitive to the $\widehat{G}_A$ mismatch, with a maximum position error of 0.867 mm in nominal condition and a barely larger 0.905 mm maximum error with +50% mismatch. Note that the result for INDI with +10% mismatch is not presented in the graph, as it is not distinguishable from the other settings.

The performance of the proposed controller is evaluated and compared to the state-of-the-art hydraulic robotic manipulator control systems reviewed in a recent survey paper [24], in which the stability guaranteed adaptive nonlinear controllers [22], [23] show the best performance. In [24], a performance indicator ρ is suggested to evaluate the performance by taking into consideration of not only the absolute error, but also the maximum velocity of the trajectory, which is defined as

$$\rho = \frac{\max\left(|\boldsymbol{x}_d - \boldsymbol{x}|\right)}{\max\left(|\dot{\boldsymbol{x}}|\right)} = \frac{|e|_{\max}}{|\dot{\boldsymbol{x}}|_{\max}}. \tag{38}$$

In Table I, the performance indicators of the proposed INDI control system in nominal and +50% parameter mismatch conditions are compared with the best performance counterparts for parallel hydraulic systems and serial manipulators concluded in the survey [24]. It is clear that the INDI control system gives almost the same performance in both nominal and parameter mismatch conditions, which have also better ρ indicator values listed than other approaches in literature. The advantage of the proposed method is even more obvious by taking the size of the systems into consideration, as the INDI controller applied to the considered SRS system achieves improved position tracking accuracy with a significantly heavier load of over 4000 kg. It can be concluded that the INDI

hydraulic control system has one of the best motion control performance of the current hydraulic robotic manipulators.

C. Motion Profile 2

A more aggressive asymmetrical motion used for a previous state estimation experiment [46] is used to further evaluate the proposed controller, with more excitation of all nonlinear dynamics and kinematics. In this motion, the upper platform traces a 0.5 m radius circular path in the horizontal plane with a period of five seconds. A periodic roll and pitch motion with an amplitude of 10 deg/s and a period of 2.5 s is superimposed on this planer movement. With maximum actuator displacement and velocity of 0.7 m and 0.7 m/s, respectively, this motion exploits up to about 60% of the total safe stroke and 70% of the maximum velocity. The force and position tracking errors of Actuator 2 with different controller settings are shown in Fig. 13. The performance of INDI with 50% mismatch is still almost identical to the nominal case, with about 2.5% maximum force error and 2.2 mm maximum position error, while for the NDI controller these are 10% and 6.5 mm for the nominal case and degraded to 20% and 11 mm with only 10% parameter offset. This result indicates that the performance of traditional feedback linearization deteriorates faster than the INDI with more aggressive motions, because more serious nonlinear effects are excited when the system exploits a larger operation space. The trajectory tracking performance in the horizontal plane is illustrated in Fig. 14. The maximum error of INDI with 50% parameter mismatch is well below 2 mm, much better than that of the NDI with 4.5 mm in nominal condition and 8 mm with 10% mismatch.

The experiment results show that high-precision hydraulic robot force/motion tracking is achieved with the proposed INDI controller even in existence of significant magnitude of parameter mismatch, without explicit use of computationally heavy adaptive or robust control algorithms. From a practical point of view, the INDI controller design procedure is straightforward and can be easily implemented for other applications.

VI. Conclusion

This paper presents the implementation of the INDI controller on a full-scale hexapod hydraulic flight simulator motion system. Acting as a hydraulic actuator force tracking controller, the proposed technique is robust against even unrealistic hydraulic parametric uncertainties and disturbances, while providing better tracking performance than a traditional feedback linearization approach. The robustness of INDI against parameter uncertainty and its stability are proven, and an estimation of parameter mismatch tolerance is given as a necessary condition for stability. Combined with a commonly applied force computation outer-loop motion controller, a high-precision motion control system is developed for the hexapod motion system of the SRS. For the implementation on this long-stroke system, solutions to practical problems, such as oil transmission line resonance effect, have been discussed comprehensively, as a guide for other real-world applications. We demonstrate a significant improvement of tracking accuracy compared with the state-of-the-art research. The simplicity of the design procedure and the low computation load makes the INDI a potential off-the-shelf control technique for other hydraulic motion systems.

Acknowledgment

The authors would like to thank the Chinese Scholarship Council (CSC) for supporting the first author.

References

[1] M. Hutter, P. Leemann, G. Hottiger, R. Figi, S. Tagmann, G. Rey, and G. Small, "Force control for active chassis balancing," *IEEE/ASME Transactions on Mechatronics*, vol. 22, no. 2, pp. 613–622, April 2017.

[2] C. Semini, V. Barasuol, J. Goldsmith, M. Frigerio, M. Focchi, Y. Gao, and D. G. Caldwell, "Design of the hydraulically actuated, torque-controlled quadruped robot hyq2max," *IEEE/ASME Transactions on Mechatronics*, vol. 22, no. 2, pp. 635–646, April 2017.

[3] T. Boaventura, J. Buchli, C. Semini, and D. G. Caldwell, "Model-based hydraulic impedance control for dynamic robots," *IEEE Transactions on Robotics*, vol. 31, no. 6, pp. 1324–1336, Dec 2015.

[4] J. Koivumäki and J. Mattila, "Stability-guaranteed impedance control of hydraulic robotic manipulators," *IEEE/ASME Transactions on Mechatronics*, vol. 22, no. 2, pp. 601–612, April 2017.

[5] O. Stroosma, M. M. van Paassen, and M. Mulder, "Using the SIMONA Research Simulator For Human-Machine Interaction Research," in *AIAA Modeling and Simulation Technologies Conference and Exhibit*, 2003.

[6] H. Abdellatif and B. Heimann, "Advanced model-based control of a 6-dof hexapod robot: A case study," *IEEE/ASME Transactions on Mechatronics*, vol. 15, no. 2, pp. 269–279, April 2010.

[7] M. Díaz-Rodríguez, A. Valera, V. Mata, and M. Valles, "Model-based control of a 3-dof parallel robot based on identified relevant parameters," *IEEE/ASME Transactions on Mechatronics*, vol. 18, no. 6, pp. 1737–1744, Dec 2013.

[8] L. Ren, J. K. Mills, and D. Sun, "Experimental comparison of control approaches on trajectory tracking control of a 3-dof parallel robot," *IEEE Transactions on Control Systems Technology*, vol. 15, no. 5, pp. 982–988, Sept 2007.

[9] P. H. Chang and J. H. Jung, "A systematic method for gain selection of robust pid control for nonlinear plants of second-order controller canonical form," *IEEE Transactions on Control Systems Technology*, vol. 17, no. 2, pp. 473–483, March 2009.

[10] J.-H. Chin, Y.-H. Sun, and Y.-M. Cheng, "Force computation and continuous path tracking for hydraulic parallel manipulators," *Control Engineering Practice*, vol. 16, no. 6, pp. 697 – 709, 2008, special Section on Large Scale Systems10th IFAC/IFORS/IMACS/IFIP Symposium on Large Scale Systems: Theory and Applications.

[11] I. Davliakos and E. Papadopoulos, "Model-based control of a 6-dof electrohydraulic stewartgough platform," *Mechanism and Machine Theory*, vol. 43, no. 11, pp. 1385 – 1400, 2008.

[12] A. Alleyne and R. Liu, "A simplified approach to force control for electro-hydraulic systems," *Control Engineering Practice*, vol. 8, no. 12, pp. 1347 – 1356, 2000.

[13] A. Alleyne, R. Liu, and H. Wright, "On the limitations of force tracking control for hydraulic active suspensions," in *Proceedings of the 1998 American Control Conference. ACC (IEEE Cat. No.98CH36207)*, vol. 1, Jun 1998, pp. 43–47 vol.1.

[14] G. Vossoughi and M. Donath, "Dynamic feedback linearization for electrohydraulically actuated control systems," *ASME. J. Dyn. Sys., Meas., Control.*, vol. 117, no. 4, pp. 468–477, 1995.

[15] A. Plummer, "Model-based motion control for multi-axis servohydraulic shaking tables," *Control Engineering Practice*, vol. 53, pp. 109 – 122, 2016.

[16] J. Heintze and A. van der Weiden, "Inner-loop design and analysis for hydraulic actuators, with an application to impedance control," *Control Engineering Practice*, vol. 3, no. 9, pp. 1323 – 1330, 1995.

[17] F. Kock and C. Ferrari, "Flatness-based high frequency control of a hydraulic actuator," *Journal of Dynamic Systems, Measurement, and Control*, vol. 134, no. 2, p. 021003, 2012.

[18] Q. Quan, G. X. Du, and K. Y. Cai, "Proportional-integral stabilizing control of a class of mimo systems subject to nonparametric uncertainties by additive-state-decomposition dynamic inversion design," *IEEE/ASME Transactions on Mechatronics*, vol. 21, no. 2, pp. 1092–1101, April 2016.

[19] Q. Quan and K. Y. Cai, "Additive-output-decomposition-based dynamic inversion tracking control for a class of uncertain linear time-invariant systems," in *2012 IEEE 51st IEEE Conference on Decision and Control (CDC)*, Dec 2012, pp. 2866–2871.
[20] B. Yao, F. Bu, J. Reedy, and G. T. C. Chiu, "Adaptive robust motion control of single-rod hydraulic actuators: theory and experiments," *IEEE/ASME Transactions on Mechatronics*, vol. 5, no. 1, pp. 79–91, Mar 2000.
[21] S. Chen, Z. Chen, B. Yao, X. Zhu, S. Zhu, Q. Wang, and Y. Song, "Adaptive robust cascade force control of 1-dof hydraulic exoskeleton for human performance augmentation," *IEEE/ASME Transactions on Mechatronics*, vol. 22, no. 2, pp. 589–600, April 2017.
[22] J. Koivumäki and J. Mattila, "High performance non-linear motion/force controller design for redundant hydraulic construction crane automation," *Automation in construction*, vol. 51, pp. 59–77, 2015.
[23] M. R. Sirouspour and S. E. Salcudean, "Nonlinear control of hydraulic robots," *IEEE Transactions on Robotics and Automation*, vol. 17, no. 2, pp. 173–182, 2001.
[24] J. Mattila, J. Koivumäki, and D. G. Caldwell, "A survey on control of hydraulic robotic manipulators with projection to future trends," *IEEE/ASME Transactions on Mechatronics*, vol. 22, no. 2, pp. 669 – 680, 2017.
[25] S. Sieberling, Q. P. Chu, and J. A. Mulder, "Robust Flight Control Using Incremental Nonlinear Dynamic Inversion and Angular Acceleration Prediction," *Journal of Guidance, Control, and Dynamics*, vol. 33, no. 6, pp. 1732–1742, nov 2010.
[26] P. Simplício, M. D. Pavel, E. van Kampen, and Q. P. Chu, "An acceleration measurements-based approach for helicopter nonlinear flight control using incremental nonlinear dynamic inversion," *Control Engineering Practice*, vol. 21, no. 8, pp. 1065 – 1077, 2013.
[27] E. J. J. Smeur, Q. P. Chu, and G. C. de Croon, "Adaptive Incremental Nonlinear Dynamic Inversion for Attitude Control of Micro Aerial Vehicles," *Journal of Guidance,Control, and Dynamics*, vol. 39, no. 3, pp. 450–461, 2016.
[28] Y. Huang, D. M. Pool, O. Stroosma, Q. P. Chu, and M. Mulder, "A Review of Control Schemes for Hydraulic Stewart Platform Flight Simulator Motion Systems," in *AIAA Modeling and Simulation Technologies Conference*, January 2016.
[29] Y. Huang, D. Pool, O. Stroosma, and Q. Chu, "Incremental nonlinear dynamic inversion control for hydraulic hexapod flight simulator motion systems," *IFAC-PapersOnLine*, vol. 50, no. 1, pp. 4294 – 4299, 2017, 20th IFAC World Congress.
[30] B. Dasgupta and T. Mruthyunjaya, "Closed-form dynamic equations of the general stewart platform through the newtoneuler approach," *Mechanism and Machine Theory*, vol. 33, no. 7, pp. 993 – 1012, 1998.
[31] Y. Huang, D. M. Pool, O. Stroosma, Q. P. Chu, and M. Mulder, "Modeling and Simulation of Hydraulic Hexapod Flight Simulator Motion Systems," in *AIAA Modeling and Simulation Technologies Conference*, January 2016.
[32] H. E. Merritt, *Hydraulic control systems*. John Wiley & Sons, 1967.
[33] J.-J. E. Slotine, W. Li *et al.*, *Applied nonlinear control*. Prentice hall Englewood Cliffs, NJ, 1991, vol. 199, no. 1.
[34] R. Da Costa, Q. Chu, and J. Mulder, "Reentry flight controller design using nonlinear dynamic inversion," *Journal of Spacecraft and Rockets*, vol. 40, no. 1, pp. 64–71, 2003.
[35] C. H. An, C. G. Atkeson, J. D. Griffiths, and J. M. Hollerbach, "Experimental evaluation of feedforward and computed torque control," *IEEE Transactions on Robotics and Automation*, vol. 5, no. 3, pp. 368–373, Jun 1989.
[36] H. K. Khalil, *Nonlinear Systems (3rd ed.)*. Prentice Hall, 2002.
[37] X. Wang, E.-J. Van Kampen, Q. P. Chu, and P. Lu, "Stability analysis for incremental nonlinear dynamic inversion control," in *2018 AIAA Guidance, Navigation, and Control Conference*.
[38] T. C. Hsia and L. S. Gao, "Robot manipulator control using decentralized linear time-invariant time-delayed joint controllers," in *Proceedings., IEEE International Conference on Robotics and Automation*, May 1990, pp. 2070–2075 vol.3.
[39] S. Koekebakker, "Model Based Control of a Flight Simulator Motion System," Ph.D. dissertation, Delft University of Technology, 2001.
[40] Q. Quan and K.-Y. Cai, "Time-domain analysis of the savitzkygolay filters," *Digital Signal Processing*, vol. 22, no. 2, pp. 238 – 245, 2012.
[41] W. C. Yang and W. E. Tobler, "Dissipative Modal Approximation of Fluid Transmission Lines Using Linear Friction Model," *Journal of Dynamic Systems, Measurement, and Control*, vol. 113, no. 1, pp. 152–162, 1991.
[42] G. van Schothorst, P. Teerhuis, and A. van der Weiden, "Stability analysis of a hydraulic servo-system including transmission line effects," in *Proceedings of the Third International conference on Automation, Robitics and Computer Vision, Singapore*, 1994, pp. 1919–1923.
[43] D. Garagic and K. Srinivasan, "Application of nonlinear adaptive control techniques to an electrohydraulic velocity servomechanism," *IEEE Transactions on Control Systems Technology*, vol. 12, no. 2, pp. 303–314, March 2004.
[44] Y. Pi and X. Wang, "Observer-based cascade control of a 6-dof parallel hydraulic manipulator in joint space coordinate," *Mechatronics*, vol. 20, no. 6, pp. 648 – 655, 2010.
[45] H. Guo, Y. Liu, G. Liu, and H. Li, "Cascade control of a hydraulically driven 6-dof parallel robot manipulator based on a sliding mode," *Control Engineering Practice*, vol. 16, no. 9, pp. 1055 – 1068, 2008.
[46] I. Miletović, D. Pool, O. Stroosma, M. van Paassen, and Q. Chu, "Improved stewart platform state estimation using inertial and actuator position measurements," *Control Engineering Practice*, vol. 62, no. Supplement C, pp. 102 – 115, 2017.

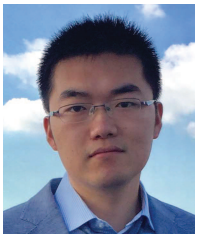

Yingzhi Huang received the B.S and M.S degrees in aeronautical control engineering from Northwestern Polytechnical University, Xi'an, China, in 2012 and 2014, respectively. Since October 2014, he has been with the section Control and Simulation, Aerospace Engineering, TU Delft, The Netherlands, where he is working towards the Ph.D. degree on the nonlinear control of the hydraulic hexapod flight simulator motion system. His research interests include control of hydraulic robotic manipulators, flight control, nonlinear control and robust control.

Daan M. Pool (M'09) received the M.Sc. and Ph.D. degrees (*cum laude*) from TU Delft, The Netherlands, in 2007 and 2012, respectively. He is currently an Assistant Professor with the section Control and Simulation, Aerospace Engineering, TU Delft. His research interests include cybernetics, manual vehicle control, simulator-based training, and mathematical modeling, identification, and optimization techniques.

Olaf Stroosma received an M.Sc. degree in Aerospace Engineering from TU Delft, The Netherlands, in 1998. He is currently a senior researcher with the section Control and Simulation, Aerospace Engineering, TU Delft, where he manages the SIMONA Research Simulator facility. His research interests include human-machine interaction, flight simulator technology, and flight control.

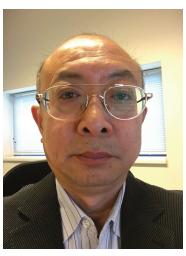

QiPing Chu received his Ph.D degree from the Faculty of Aerospace Engineering, TU Delft in 1987. He is presently an associate professor and the head of Aerospace Guidance, Navigation and Control Cluster at the Section of Control and Simulation, Faculty of Aerospace Engineering, TU Delft. The research interests of Dr. Chu are nonlinear control, adaptive control, system identification and state estimation with applications to fault tolerant control, sensor integration, data analysis, and fault detection/diagnosis.